

Effective anisotropic interaction potentials for pairs of ultracold molecules shielded by a static electric field

Bijit Mukherjee*

Faculty of Physics, University of Warsaw, Pasteura 5, 02-093 Warsaw, Poland

Luis Santos

Institut für Theoretische Physik, Leibniz Universität Hannover, Appelstrasse 2, D-30167 Hannover, Germany

Jeremy M. Hutson†

*Joint Quantum Centre (JQC) Durham-Newcastle, Department of Chemistry,
Durham University, South Road, Durham, DH1 3LE, United Kingdom.*

(Dated: July 8, 2025)

Quantum gases of ultracold polar molecules have novel properties because of the strong dipolar forces between molecules. Current experiments shield the molecules from destructive collisions by engineering long-range repulsive interactions using microwave or static electric fields. These shielding methods produce interaction potentials with large repulsive cores that are not well described with contact potentials. In this paper we explore the anisotropic interaction potentials that arise for pairs of polar molecules shielded with static electric fields. We derive computationally inexpensive approximations for the potentials that are suitable for use in calculations of many-body properties. The interaction potentials for molecules shielded with static fields are qualitatively different from those that arise from single-field microwave shielding and will produce quite different many-body physics.

I. INTRODUCTION

Recent advances in experiment and theory for ultracold molecules have led to the production of Fermi-degenerate gases [1–4] and Bose-Einstein condensates [5] of polar molecules. These advances open new frontiers in the physics of dipolar gases. Molecules with permanent electric dipole moments can produce much stronger dipole-dipole interactions than magnetic atoms [6]. Molecular dipoles are generally weaker than those of Rydberg atoms [7], but ultracold polar molecules can have long lifetimes and coherence times [8] that are hard to achieve for Rydbergs.

Left to themselves, ultracold polar molecules do not stay trapped for long. They undergo collisions with one another that result in trap loss. The loss is not fully understood [9], but is believed to occur via formation of 2-molecule collision complexes [10] followed by excitation due to the trapping laser [11]. In any case, the loss can be effectively prevented by *shielding* methods, which engineer long-range potential barriers to prevent colliding pairs reaching short range, where the losses occur.

There are two types of shielding in current use. Static-field shielding [12–17] engineers the repulsive barrier by using a strong electric field to tune close to a 2-molecule degeneracy, and the dipole-dipole interaction then produces a repulsive barrier in the effective potential for the shielded state. Microwave shielding [18–24] engineers an analogous repulsive barrier by using microwave radiation,

blue-detuned from a molecular rotational transition, to create a similar near-degeneracy.

For either type of shielding, the interaction between molecules is characterized by an effective interaction potential that is very different from that for magnetic atoms, and also different from that assumed in most theories of dipolar gases. The major difference is that, for magnetic atoms, repulsion occurs at very short range (around 10 bohr). Such repulsive interactions are fairly well represented with zero-range contact potentials modeled with Dirac delta-functions. This is the formulation used, for example, in the widely used theoretical *ansatz* of Yi and You [25, 26]. However, the interactions between shielded molecules are characterized by a very large repulsive core. The excluded volume corresponds to a range of order 1000 bohr [13, 17, 18]. For the large repulsive cores encountered for shielded molecules, a contact potential is a very poor approximation. This is likely to produce very different many-body physics [27–29].

To simulate many-body properties of systems made up of shielded ultracold molecules, we need simple representations of the effective potentials involved. For molecules shielded by a single microwave field [18], suitable potentials have been provided by Deng *et al.* [24] and used for many-body simulations [27]. In the microwave case the potentials are antidipolar at long range, meaning that they are repulsive for end-to-end approach of two molecules and attractive for side-to-side approach. At shorter range (inside a few hundred bohr), there is a repulsive potential that is itself strongly anisotropic.

For molecules shielded by static fields, the long-range potentials are qualitatively different from those for single-field microwave shielding. They are similar to those for dipoles fixed in space, and are attractive for end-to-end

* bijit.9791@gmail.com

† j.m.hutson@durham.ac.uk

approach and repulsive for side-to-side approach. This is likely to lead to very different behaviour for many-body systems. Nevertheless, the effective potentials still have large repulsive cores [16, 17] and these are highly anisotropic. In this paper we investigate the anisotropic interaction potentials for molecules shielded by static fields and derive computationally inexpensive approximate forms for them that are suitable for quantum many-body calculations.

II. THEORY

A. Hamiltonian and its matrix elements

We follow a theoretical approach similar to that in ref. [16]. The Hamiltonian for a single polar molecule in a 1Σ state, in the presence of an electric field \mathbf{F} , is

$$\hat{h} = b\hat{n}^2 - \boldsymbol{\mu} \cdot \mathbf{F}, \quad (1)$$

where \hat{n} is the operator for molecular rotation, b is the rotational constant, and $\boldsymbol{\mu}$ is the dipole moment along the molecular axis.

The Hamiltonian for a colliding pair of molecules is

$$\hat{H} = -\frac{\hbar^2}{2\mu_{\text{red}}}\hat{\nabla}^2 + \hat{h}_1 + \hat{h}_2 + \hat{H}_{\text{dd}}, \quad (2)$$

where μ_{red} is the reduced mass, $\hat{\nabla}^2$ is the Laplacian, \hat{h}_k is the Hamiltonian of molecule k from Eq. 1, and \hat{H}_{dd} represents the dipole-dipole interaction between the pair of molecules.

The dipole-dipole operator is

$$\hat{H}_{\text{dd}} = \frac{\boldsymbol{\mu}_1 \cdot \boldsymbol{\mu}_2 - 3(\boldsymbol{\mu}_1 \cdot \hat{\mathbf{R}})(\boldsymbol{\mu}_2 \cdot \hat{\mathbf{R}})}{4\pi\epsilon_0 R^3}, \quad (3)$$

where $\boldsymbol{\mu}_k$ is the dipole moment of molecule k and \mathbf{R} is the intermolecular vector, with corresponding unit vector $\hat{\mathbf{R}}$ and length R . In a spherical tensor representation,

$$\hat{H}_{\text{dd}} = -\sqrt{6}\frac{\mu_1\mu_2}{4\pi\epsilon_0 R^3} \sum_p (-1)^p [\hat{\mathbf{r}}_1 \otimes \hat{\mathbf{r}}_2]_{2,p} C_{2,-p}(\theta, \phi), \quad (4)$$

where $\hat{\mathbf{r}}_k$ is a unit vector along the axis of molecule k . Here, the functions $C_{k,p}(\theta, \phi)$ are the Racah-normalised spherical harmonics and θ and ϕ indicate the orientation of $\hat{\mathbf{R}}$ with respect to the laboratory-frame axis Z . The tensor component $[\hat{\mathbf{r}}_1 \otimes \hat{\mathbf{r}}_2]_{2,p}$ is

$$[\hat{\mathbf{r}}_1 \otimes \hat{\mathbf{r}}_2]_{2,p} = \sqrt{5} \sum_{p_1, p_2} (-1)^p \begin{pmatrix} 2 & 1 & 1 \\ p & -p_1 & -p_2 \end{pmatrix} \times C_{1,p_1}(\beta_1, \alpha_1) C_{1,p_2}(\beta_2, \alpha_2). \quad (5)$$

The angles (β_k, α_k) indicate the orientation of $\hat{\mathbf{r}}_k$ in the laboratory frame.

In a basis set of spherical harmonics for two freely rotating molecules, $|n_1, m_1; n_2, m_2\rangle$, where m is the projection of n onto the space-fixed axis Z , the matrix elements of \hat{H}_{dd} are

$$\begin{aligned} & \langle n_1, m_1; n_2, m_2 | \hat{H}_{\text{dd}} | n'_1, m'_1; n'_2, m'_2 \rangle \\ &= -\sqrt{30} \frac{\mu_1 \mu_2}{4\pi\epsilon_0 R^3} \begin{pmatrix} 2 & 1 & 1 \\ p & -p_1 & -p_2 \end{pmatrix} \langle n_1, m_1 | C_{1,p_1} | n'_1, m'_1 \rangle \\ & \times \langle n_2, m_2 | C_{1,p_2} | n'_2, m'_2 \rangle C_{2,-p}(\theta, \phi), \end{aligned} \quad (6)$$

where $p_1 = m_1 - m'_1$, $p_2 = m_2 - m'_2$ and $p = p_1 + p_2$.

We expand Eq. (6) to obtain

$$\begin{aligned} & \langle n_1, m_1; n_2, m_2 | \hat{H}_{\text{dd}} | n'_1, m'_1; n'_2, m'_2 \rangle \\ &= (-1)^{1+m_1+m_2} \sqrt{30} \frac{\mu_1 \mu_2}{4\pi\epsilon_0 R^3} \begin{pmatrix} 2 & 1 & 1 \\ p & -p_1 & -p_2 \end{pmatrix} C_{2,-p}(\theta, \phi) \\ & \times \sqrt{(2n_1+1)(2n'_1+1)} \begin{pmatrix} n_1 & 1 & n'_1 \\ -m_1 & p_1 & m'_1 \end{pmatrix} \begin{pmatrix} n_1 & 1 & n'_1 \\ 0 & 0 & 0 \end{pmatrix} \\ & \times \sqrt{(2n_2+1)(2n'_2+1)} \begin{pmatrix} n_2 & 1 & n'_2 \\ -m_2 & p_2 & m'_2 \end{pmatrix} \begin{pmatrix} n_2 & 1 & n'_2 \\ 0 & 0 & 0 \end{pmatrix}. \end{aligned} \quad (7)$$

In the presence of an external static electric field F along Z , the rotational states are field-dressed due to the Stark interaction. They are denoted $|\tilde{n}, m\rangle$ and correlate at zero field to free-rotor states $|n, m\rangle$. The projection m is conserved and

$$|\tilde{n}, m\rangle = \sum_n c_{n\tilde{n}}^m(F) |n, m\rangle. \quad (8)$$

The matrix elements of the single-molecule dipole operator between the field-dressed functions are

$$\begin{aligned} d_{\tilde{n}m, \tilde{n}'m'}(F) &= (-1)^m \mu \sum_{nn'} c_{n\tilde{n}}^m c_{n'\tilde{n}'}^{m'} \sqrt{(2n+1)(2n'+1)} \\ & \times \begin{pmatrix} n & 1 & n' \\ -m & m-m' & m' \end{pmatrix} \begin{pmatrix} n & 1 & n' \\ 0 & 0 & 0 \end{pmatrix}. \end{aligned} \quad (9)$$

The matrix elements of \hat{H}_{dd} in the field-dressed rotor pair basis set are

$$\begin{aligned} & \langle \tilde{n}_1, m_1; \tilde{n}_2, m_2 | \hat{H}_{\text{dd}} | \tilde{n}'_1, m'_1; \tilde{n}'_2, m'_2 \rangle \\ &= -\frac{\sqrt{30} d_{\tilde{n}_1 m_1, \tilde{n}'_1 m'_1} d_{\tilde{n}_2 m_2, \tilde{n}'_2 m'_2}}{4\pi\epsilon_0 R^3} \begin{pmatrix} 2 & 1 & 1 \\ p & -p_1 & -p_2 \end{pmatrix} C_{2,-p}(\theta, \phi). \end{aligned} \quad (10)$$

For identical molecules, the rotor pair functions are symmetrised with respect to exchange,

$$\begin{aligned} |\tilde{n}_1, m_1; \tilde{n}_2, m_2\rangle^\pm &= [2(1 + \delta_{\tilde{n}_1 \tilde{n}_2} \delta_{m_1 m_2})]^{-1/2} \\ & \times (|\tilde{n}_1, m_1; \tilde{n}_2, m_2\rangle \pm |\tilde{n}_2, m_2; \tilde{n}_1, m_1\rangle). \end{aligned} \quad (11)$$

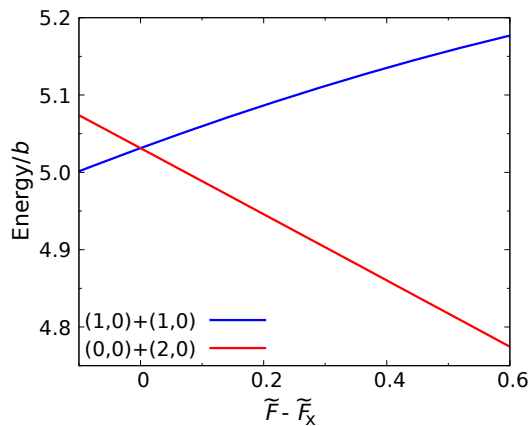


FIG. 1. The crossing of pair states $(1,0)+(1,0)$ and $(0,0)+(2,0)$ that gives rise to static-electric field shielding. $(1,0)+(1,0)$ is the initial pair state of the molecules. Energies and fields are shown in dimensionless units; in this form the figure applies to any linear molecule in a $^1\Sigma$ state, with $\tilde{F}_X = 3.244$.

If the two molecules are initially in the same state, as is usual for shielding, only the + linear combination contributes. This is true for either bosons or fermions.

In a full treatment of molecular collisions [16], we construct basis functions that are products of rotor pair functions $|\tilde{n}_1, m_1; \tilde{n}_2, m_2\rangle^\pm$ and partial-wave functions $|L, M_L\rangle$. Expanding the total Schrödinger equation in this basis set gives a set of coupled-channel equations. These may be solved as in ref. [16] to produce S-matrices, scattering lengths and cross sections for elastic scattering and 2-body loss. In the present work, however, we bypass coupled-channel calculations and focus instead on effective potentials as described below.

B. Shielding with a static electric field

For collisions shielded by a static electric field, it is convenient to represent the field by a dimensionless quantity $\tilde{F} = F\mu/b$ [14], where b is the rotational constant of the molecule. Similarly, the molecular energies are expressed in units of b . The pair state $(\tilde{n}_1, m_1)+(\tilde{n}_2, m_2) = (1,0)+(1,0)$ crosses $(0,0)+(2,0)$ at a critical electric field $\tilde{F}_X = 3.244$, as shown in Fig. 1. At fields $\tilde{F} > \tilde{F}_X$, $(1,0)+(1,0)$ lies above $(0,0)+(2,0)$, and thus experiences repulsion due to interaction with it via \hat{H}_{dd} . This gives rise to *shielding* for the initial pair state $(1,0)+(1,0)$.

For two dipoles fixed in space, the coupled equations may be cast in dimensionless form [30]. Here we choose to express lengths in terms of a dipole length $R_3 = (2\mu_{\text{red}}/\hbar^2)(\mu^2/4\pi\epsilon_0)$ and energies in terms of a corresponding energy $E_3 = \hbar^2/(2\mu_{\text{red}}R_3^2)$. However, static-field shielding arises from mixing of rotational states. At a particular value of \tilde{F} , *all* the separations between

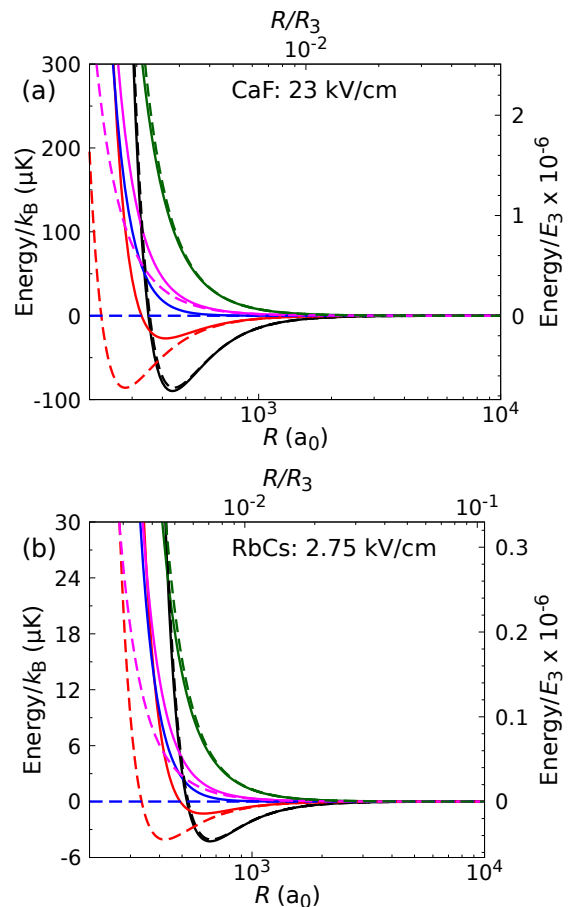


FIG. 2. The adiabats that correspond to the initial pair state $(1,0)+(1,0)$ for (a) CaF and (b) RbCs at electric field $\tilde{F} = 3.46$. Solid lines are obtained from full matrix diagonalisation whereas dashed lines are obtained by diagonalising the matrix of Eq. 12.

different rotor states are proportional to b , or in reduced units to $\tilde{b} = b/E_3$. This includes the separation between $(1,0)+(1,0)$ and $(0,0)+(2,0)$. Because of this, static-field shielding depends crucially on \tilde{b} , which ranges from $\sim 10^6$ for NaLi to $\sim 10^{11}$ for YO [14]. Molecules with $\tilde{b} > 10^9$ show effective shielding properties at fields $\tilde{F}_X < \tilde{F} < \tilde{F}_X + 0.6$. Some molecules with smaller \tilde{b} are still promising for shielding but at fields in a somewhat smaller range [14, 17]. In the following, we consider effective potentials for both CaF (with $\tilde{b} = 4.1 \times 10^9$) and RbCs (with $\tilde{b} = 2.6 \times 10^8$) to illustrate the differences that arise.

We begin by constructing a basis set of field-dressed rotor pair functions $|\tilde{n}_1, m_1; \tilde{n}_2, m_2\rangle^+$, including functions up to $n_{\text{max}} = \tilde{n}_{\text{max}} = 5$ for each molecule. This gives good numerical convergence. Diagonalising the Hamiltonian matrix formed from $\hat{h}_1 + \hat{h}_2 + \hat{H}_{dd}$ in this basis set produces adiabats (effective potentials) that are functions of R and θ . There is no dependence on ϕ because

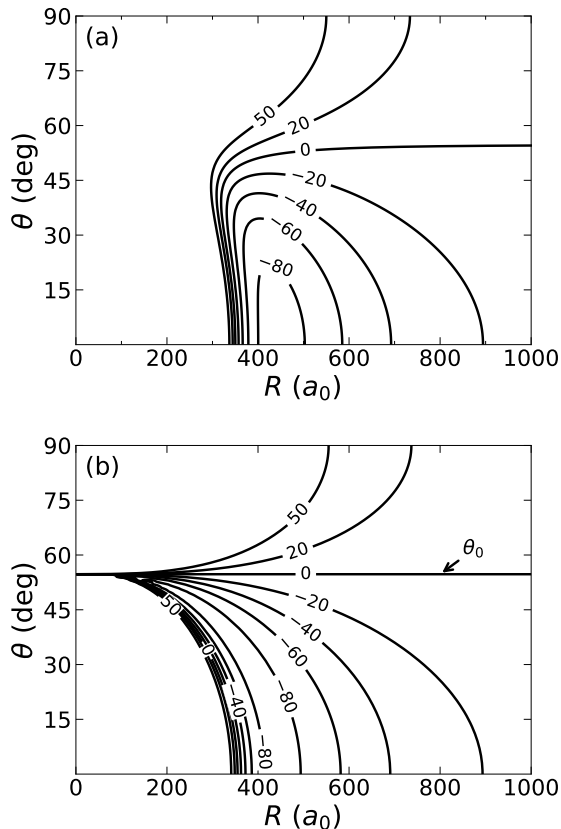


FIG. 3. Contour plots of adiabats obtained from (a) full matrix diagonalisation, and (b) diagonalising the matrix of Eq. 12 for CaF at $F = 23$ kV/cm. Contours are labeled in μK and shown only up to $50 \mu\text{K}$.

the two-molecule system is cylindrically symmetric in the presence of an electric field. Adiabats corresponding to the initial pair state $(1,0)+(1,0)$ for CaF and RbCs are shown as solid lines in Fig. 2 for a field where shielding is effective. The results for CaF are shown as a contour plot in Fig. 3(a). The effective potentials are repulsive inside $R \sim 300 a_0$ at all angles, but are attractive at long range for angles $\theta < \theta_0$, where $\theta_0 = \cos^{-1}(1/\sqrt{3}) \approx 55^\circ$ is the semi-tetrahedral angle where the first-order dipole-dipole interaction vanishes.

The effective potentials are qualitatively similar for CaF and RbCs, but the positions and depths of the potential wells are quite different in reduced units. In these units the first-order dipole-dipole part of the potential is the same for the two species, but the shielding repulsion is approximately proportional to $1/\tilde{b}$. As a result, the potential wells for CaF are much deeper and occur at much shorter range than those for RbCs in reduced units.

III. ANALYTIC EFFECTIVE POTENTIALS

Our goal is to obtain a simple approximate form of the effective potential for the initial pair state $(1,0)+(1,0)$, avoiding diagonalisation of substantial matrices. We first consider a 2×2 Hamiltonian matrix that involves only the pair states $(1,0)+(1,0)$ and $(0,0)+(2,0)$, here denoted 1 and 2, respectively. These are the states that produce the main shielding effect at most angles. Using Eq. 10, the matrix elements may be written

$$H_{11} = -\frac{2(d_{10,10})^2}{4\pi\epsilon_0 R^3} P_2(\cos \theta), \quad (12a)$$

$$H_{12} = -\frac{2\sqrt{2}d_{00,10}d_{10,20}}{4\pi\epsilon_0 R^3} P_2(\cos \theta), \quad (12b)$$

$$H_{22} = -\frac{2(d_{00,00}d_{20,20} + (d_{00,20})^2)}{4\pi\epsilon_0 R^3} P_2(\cos \theta) - \Delta, \quad (12c)$$

where $P_2(\cos \theta) = \frac{1}{2}(3\cos^2 \theta - 1)$. The matrix elements $d_{\tilde{n}m, \tilde{n}'m'}$ and the energy separation Δ between states 1 and 2 are functions of field.

Lassablière and Quémener [31] obtained effective potentials by diagonalising the 2×2 matrix of Eq. 12. The resulting adiabats are shown as dashed lines for CaF and RbCs in Fig. 2. Figure 3(b) shows the results for CaF as a contour plot. It may be seen that the potentials of ref. [31] are accurate at $\theta = 0$ and 90° , but show no attraction or repulsion at the semi-tetrahedral angle θ_0 , where $P_2(\cos \theta) = 0$. They produce attractive wells that are substantially too deep and at much too short range at angles just below $\theta = \theta_0$. These properties would be likely to produce unphysical artefacts in simulations of many-body properties.

To overcome this limitation, it is necessary to include additional pair states that provide repulsion around $\theta = \theta_0$. These are energetically further away and we take them into account through either second-order perturbation theory or a Van Vleck transformation.

In the present work, we first describe a minimal model for the effective potential in Sec. III A, using second-order perturbation theory in a limited basis set. Subsequently, in Sec. III B, we describe a more accurate treatment, based on Van Vleck perturbation theory in a larger basis set, that is only slightly more complicated to evaluate and gives accurate results.

A. Perturbative model

We obtain an effective potential using a perturbative model $V_{\text{eff}}^{\text{pert}}$ by considering the initial pair state $(1,0)+(1,0)$ only and treating the most important additional pair states using second-order perturbation theory.

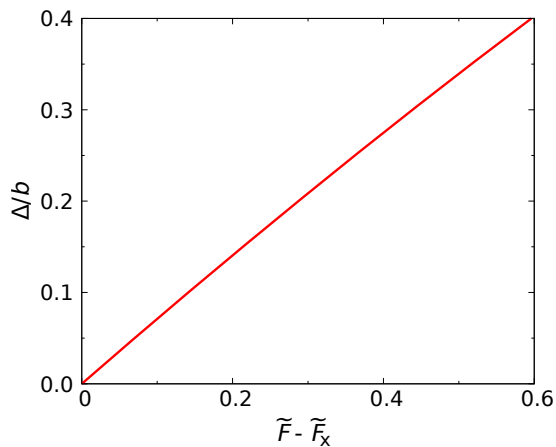


FIG. 4. The energy separation between pair states $(1,0)+(1,0)$ and $(0,0)+(2,0)$. The field range is chosen where shielding is effective.

We write this effective potential as

$$V_{\text{eff}}^{\text{pert}}(R, \theta) = H_{11}(R, \theta) + \frac{|H_{12}(R, \theta)|^2}{H_{11} - H_{22}} + V_{\text{rest}}(R, \theta). \quad (13)$$

The second term represents the repulsion due to the lower-lying level $(0,0)+(2,0)$, while $V_{\text{rest}}(R, \theta)$ takes account of the interaction due to other pairs. In this model, both of these are treated perturbatively.

We formulate the effective potential for fields $\tilde{F} < \tilde{F}_X + 0.6$, where shielding is effective for molecules such as CaF. For RbCs, the range of effective shielding is somewhat smaller, extending up to $\tilde{F}_X + 0.4$.

At most fields, the matrix elements of \hat{H}_{dd} are much smaller than the asymptotic separation Δ between states 1 and 2. We therefore make the approximation

$$H_{11} - H_{22} \approx \Delta. \quad (14)$$

Figure 4 shows that Δ is very close to linear in $\tilde{F} - \tilde{F}_X$ in the field range where shielding is effective. We therefore write

$$\Delta/b \approx \delta(\tilde{F} - \tilde{F}_X), \quad (15)$$

with slope $\delta = 0.684$.

The dipole moments for the monomer states $(\tilde{n}, m_n) = (0,0)$, $(1,0)$ and $(2,0)$, and the transition dipole moments appearing in the matrix elements of Eqs. 12 are shown in Fig. 5. For simplicity, we denote the dipole matrix elements d_{i_0, j_0} as d_{ij} . As seen in Fig. 5, these are approximately linear functions of F in the region of interest, so we approximate each of them as

$$d_{ij}/\mu \approx d_{ij}^{(0)} + d_{ij}^{(1)}(\tilde{F} - \tilde{F}_X), \quad (16)$$

with the coefficients given in Table I.

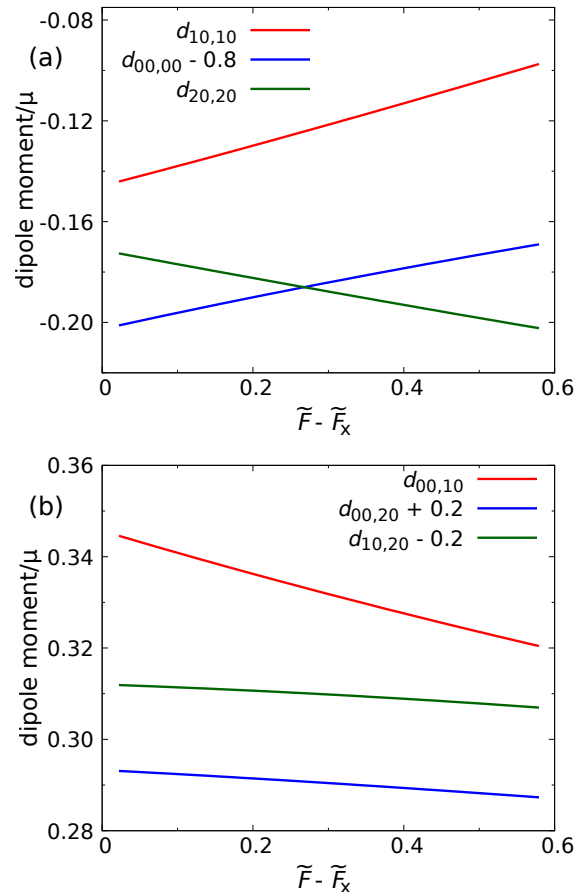


FIG. 5. The single-molecule dipole matrix elements that appear in the dipole-dipole matrix elements of Eq. 12. The blue curves in both panels and the green curve in (b) are shifted to fit within the scales of the figures.

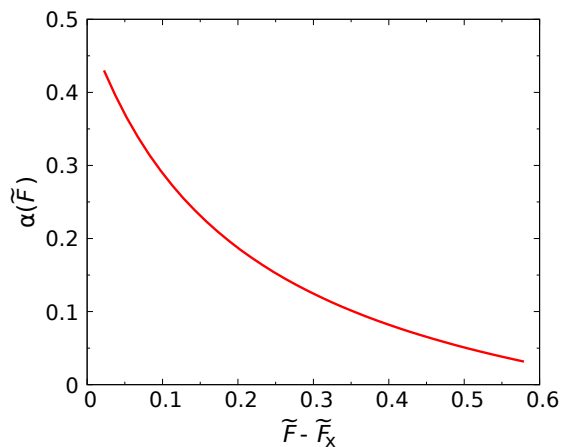


FIG. 6. Functional form of $\alpha(\tilde{F})$.

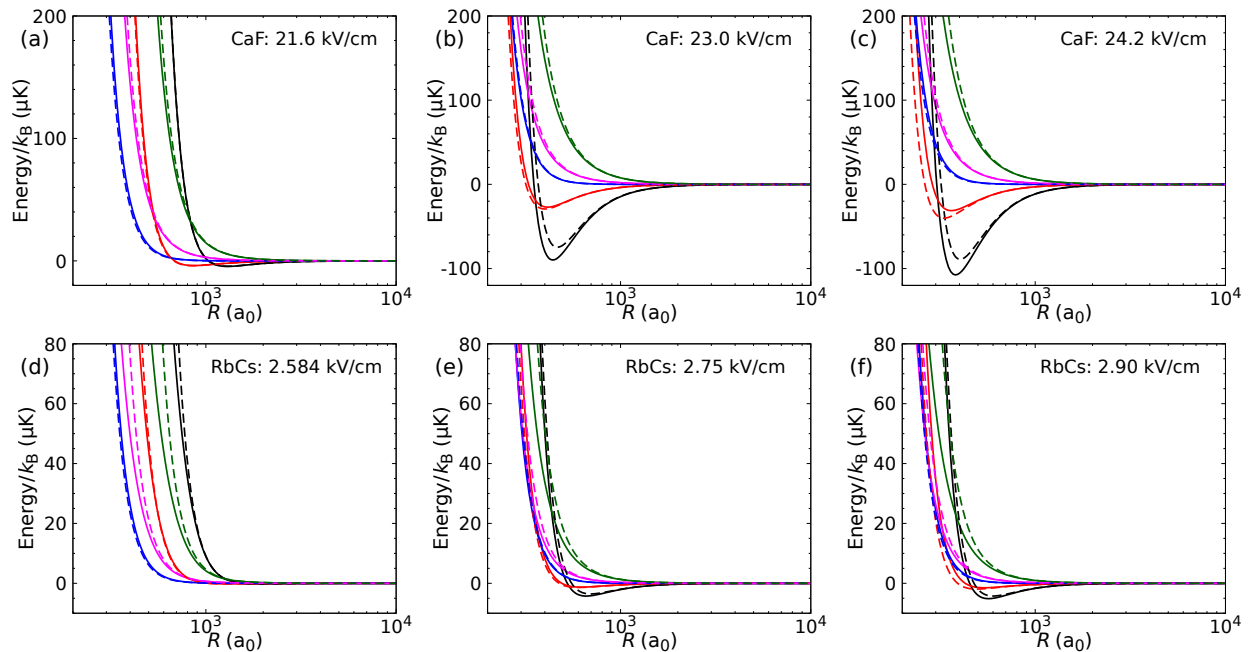


FIG. 7. Comparison of adiabats for CaF and RbCs in the initial pair state $(1,0)+(1,0)$, obtained from the perturbative model of Eq. 20 (dashed lines) and from full matrix diagonalisation (solid lines). The values of \tilde{F} correspond to (a) and (d) 3.25; (b) and (e) 3.46; and (c) and (e) 3.65.

TABLE I. The parameters defining the effective potentials obtained from the perturbative model of Eq. 20, and the coupled model of Eq. 27.

Parameter	Value
δ	0.684
$d_{00}^{(0)}$	0.598
$d_{00}^{(1)}$	0.058
$d_{11}^{(0)}$	-0.146
$d_{11}^{(1)}$	0.084
$d_{22}^{(0)}$	-0.172
$d_{22}^{(1)}$	-0.053
$d_{01}^{(0)}$	0.345
$d_{01}^{(1)}$	-0.043
$d_{02}^{(0)}$	0.093
$d_{02}^{(1)}$	-0.010
$d_{12}^{(0)}$	0.512
$d_{12}^{(1)}$	-0.009
$\alpha^{(0)}$	0.428
$\alpha^{(1)}$	-1.417
$\alpha^{(2)}$	1.315

represented as

$$V_{\text{rest}}(R, \theta) = \sum_k \frac{|H_{1k}|^2}{E_1 - E_k}. \quad (17)$$

This is smaller than the first two terms of Eq. 13 at most θ , except near $\theta = \theta_0$, where both H_{11} and H_{12} vanish. In the perturbative model, for simplicity, we therefore evaluate V_{rest} only at $\theta = \theta_0$ and use the result at all θ . At $\theta = \theta_0$, pair states with $m'_1 + m'_2 = 0$ make no contribution and $V_{\text{rest}}(R)$ is dominated by a repulsive interaction due to $(0,0)+(2,\pm 1)$, which is the pair state that lies closest to (and below) $(0,0)+(2,0)$ at these fields. All the state separations are proportional to the rotational constant b except for a weak dependence on R . With this approximation,

$$V_{\text{rest}}(R) \equiv V_{\text{rest}}(R, \theta_0) = \frac{\mu^4}{(4\pi\epsilon_0)^2 R^6} \frac{\alpha}{b}. \quad (18)$$

The dimensionless function $\alpha(\tilde{F})$ is shown in Fig. 6. We approximate it as a quadratic function of F ,

$$\alpha(\tilde{F}) \approx \alpha^{(0)} + \alpha^{(1)}(\tilde{F} - \tilde{F}_X) + \alpha^{(2)}(\tilde{F} - \tilde{F}_X)^2, \quad (19)$$

with the coefficients given in Table I.

Finally, we write the expression for the effective potential from Eq. 13 as

$$V_{\text{eff}}^{\text{pert}}(R, \theta) = \frac{C_3(\theta)}{R^3} + \frac{C_6(\theta)}{R^6}, \quad (20)$$

The contribution $V_{\text{rest}}(R, \theta)$ from other pair states k is

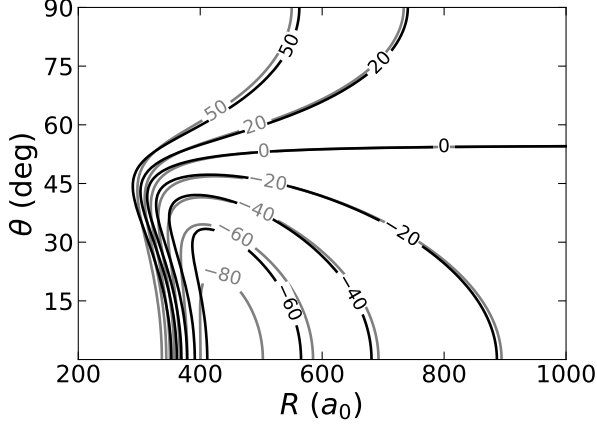


FIG. 8. Contour plot comparing $V_{\text{eff}}^{\text{pert}}$ (black lines) with adiabats obtained from full matrix diagonalisation (grey lines) for CaF at $F = 23$ kV/cm. Contours are labeled in μK and shown only up to $50 \mu\text{K}$.

where the coefficients are

$$C_3(\theta) = -\frac{2d_{11}^2}{4\pi\epsilon_0} P_2(\cos\theta), \quad (21)$$

and

$$C_6(\theta) = \frac{1}{(4\pi\epsilon_0)^2} \left(\frac{8[d_{01}d_{12}P_2(\cos\theta)]^2}{\Delta} + \frac{\alpha\mu^4}{b} \right), \quad (22)$$

with $\Delta(\tilde{F})$, $d_{ij}(\tilde{F})$ and $\alpha(\tilde{F})$ from Eqs. 15, 16 and 19, respectively.

Figure 7 compares the perturbative model with adiabats obtained from full matrix diagonalisation. Results are shown for CaF and RbCs in the initial pair state (1,0)+(1,0) at three different fields where shielding is effective. Figure 8 shows the comparison for CaF at 23 kV/cm as contour plots.

The perturbative model reproduces the qualitative features of the adiabats well. It corrects the main deficiency of Fig. 3(b) without significant extra computational expense. However, it produces some quantitative errors that may be significant in precise work. Its main deficiency is that it approximates the effect of pair states with $m'_1 + m'_2 \neq 0$ as isotropic and neglects entirely the effects of pair states other than (0,0)+(2,0) with $m'_1 + m'_2 = 0$. This approximation becomes more serious at larger \tilde{F} , where the effects of (0,0)+(2,0) are not so strongly dominant. As seen in Fig. 7, it can cause underestimates of up to 20% in well depths at higher fields. It also starts to break down at small distances when the off-diagonal matrix element H_{12} in Eq. 12 is comparable to the energy separation Δ between pair states 1 and 2. However, this occurs only for fields very close to F_X and is most significant for molecules with small values of b . It may be seen in the lowest-field panels in Fig. 7 (for

$\tilde{F} = 3.25$); the repulsion at angles different from θ_0 is overestimated for RbCs at 2.584 kV/cm but is reasonably accurate for CaF at 21.6 kV/cm.

B. Fully coupled model

The perturbative model described in section III A gives qualitatively correct results, but with some deviations from full diagonalisation. To improve on it, we need to consider the effects of additional pair states. We do this using Van Vleck perturbation theory [32, 33]. In this approach, the full set of basis functions is partitioned into two classes, denoted class 1 (labels i, j, \dots) and class 2 (labels α, β, \dots). The most important functions are in class 1 and no function in class 2 is close in energy to any function in class 1. The functions in class 1 are included explicitly in matrix diagonalisations, while those in class 2 are included perturbatively. This produces matrix elements between different functions in class 1 of the form

$$\begin{aligned} \langle i | \hat{H}_{\text{dd},\text{VV}} | j \rangle &= \sum_{\alpha} \frac{1}{2} \left[\frac{\langle i | \hat{H}_{\text{dd}} | \alpha \rangle \langle \alpha | \hat{H}_{\text{dd}} | j \rangle}{(E_i - E_{\alpha})} + \frac{\langle i | \hat{H}_{\text{dd}} | \alpha \rangle \langle \alpha | \hat{H}_{\text{dd}} | j \rangle}{(E_j - E_{\alpha})} \right]. \end{aligned} \quad (23)$$

Since \hat{H}_{dd} is proportional to R^{-3} , $\hat{H}_{\text{dd},\text{VV}}$ is proportional to R^{-6} .

In the fully coupled model, we consider the pair functions (1,0)+(1,0) and (0,0)+(2,0) in class 1, and all remaining rotor pairs in class 2. The matrix elements involving states 1 and 2, without the Van Vleck contributions, are given in Eq. 12. We model the matrix elements arising from the Van Vleck transformation as

$$\begin{aligned} H_{ij,\text{VV}}(R, \theta, \tilde{F}) &= \frac{\mu^4}{(4\pi\epsilon_0)^2 R^6} \frac{1}{b} \left[P_{ij}(\tilde{F})(1 - 3\cos^2\theta)^2 \right. \\ &\quad \left. + Q_{ij}(\tilde{F})\sin^2\theta\cos^2\theta + R_{ij}(\tilde{F})\sin^4\theta \right], \end{aligned} \quad (24)$$

with $(i, j) = (1, 1), (2, 2)$ and $(1, 2)$. The first term in square brackets represents second-order matrix elements of H_{dd} between (1,0)+(1,0) and pair states in class 2 with $|m'_1 + m'_2| = 0$. These are proportional to the square of the spherical harmonics $|C_{2,0}(\theta, \phi)|^2$. Similarly, the second and third terms represent second-order interactions with class 2 levels with $|m'_1 + m'_2| = 1$ and 2, respectively, and are proportional to $|C_{2,\pm 1}(\theta, \phi)|^2$ and $|C_{2,\pm 2}(\theta, \phi)|^2$. The coefficients $P(\tilde{F})$, $Q(\tilde{F})$ and $R(\tilde{F})$ are dimensionless functions of field, and are approximated as

$$P_{ij}(\tilde{F}) \approx P_{ij}^{(0)} + P_{ij}^{(1)}(\tilde{F} - \tilde{F}_X); \quad (25a)$$

$$Q_{ij}(\tilde{F}) \approx Q_{ij}^{(0)} + Q_{ij}^{(1)}(\tilde{F} - \tilde{F}_X) + Q_{ij}^{(2)}(\tilde{F} - \tilde{F}_X)^2; \quad (25b)$$

$$R_{ij}(\tilde{F}) \approx R_{ij}^{(0)} + R_{ij}^{(1)}(\tilde{F} - \tilde{F}_X) \quad (25c)$$

TABLE II. The fitted values of the parameters in Eqs. 25.

Parameter	Value
$P_{11}^{(0)}$	-1.76×10^{-2}
$P_{11}^{(1)}$	-2.90×10^{-3}
$P_{22}^{(0)}$	1.46×10^{-2}
$P_{22}^{(1)}$	-2.11×10^{-3}
$P_{12}^{(0)}$	-1.14×10^{-2}
$P_{12}^{(1)}$	2.76×10^{-3}
$Q_{11}^{(0)}$	2.07
$Q_{11}^{(1)}$	-6.31
$Q_{11}^{(2)}$	5.92
$Q_{22}^{(0)}$	1.95×10^{-1}
$Q_{22}^{(1)}$	1.44×10^{-1}
$Q_{22}^{(2)}$	1.90×10^{-2}
$Q_{12}^{(0)}$	-4.45×10^{-1}
$Q_{12}^{(1)}$	5.22×10^{-1}
$Q_{12}^{(2)}$	-5.19×10^{-1}
$R_{11}^{(0)}$	-7.36×10^{-2}
$R_{11}^{(1)}$	-3.36×10^{-2}
$R_{22}^{(0)}$	2.08×10^{-2}
$R_{22}^{(1)}$	-1.90×10^{-2}
$R_{12}^{(0)}$	-4.44×10^{-2}
$R_{12}^{(1)}$	-3.08×10^{-3}

with the coefficients given in Table II.

We supplement the matrix elements H_{ij} of Eq. 12 with the Van Vleck matrix elements of Eq. 24 to form a 2×2 matrix M with elements

$$M_{ij} = H_{ij} + H_{ij,vv}. \quad (26)$$

The effective potential for $(1,0)+(1,0)$ in the fully coupled model is the higher of the two eigenvalues of M ,

$$V_{\text{eff}}^{\text{fc}}(R, \theta) = \frac{1}{2}(M_{11} + M_{22}) + \frac{1}{2}\sqrt{(M_{11} - M_{22})^2 + 4M_{12}^2}, \quad (27)$$

where all the matrix elements are functions of R , θ and \vec{F} .

The fully coupled model does not involve any approximations other than the linearisation of the field-dependence of the matrix elements and the Van Vleck treatment itself. Figure 9 compares $V_{\text{eff}}^{\text{fc}}$ with the full adiabats for CaF and RbCs, while Fig. 10 shows the results for CaF at 23 kV/cm as contour plots. The agreement is excellent, and of similar quality for CaF and RbCs.

IV. CONTRAST WITH MICROWAVE SHIELDING

The effective potentials for static-field shielding may be contrasted with those for microwave shielding with a

circularly polarised field [24]. The range and depth of the potentials depend strongly on microwave Rabi frequency and detuning, but examples are shown in Fig. 11 for conditions that are reasonable for CaF. The potentials are attractive at long range for angles $\theta_0 < \theta < 180^\circ - \theta_0$, but repulsive at all distances for $\theta < \theta_0$. This is opposite to the situation for static-field shielding. Both static-field and microwave shielding provide large repulsive cores that are very different from the short-range (contact-like) interactions that are common in atomic systems. However, the dipole-dipole forces resulting from static-field shielding favour geometries around $\theta = 0$, while those from microwave shielding with circular polarisation favour geometries around $\theta = 90^\circ$.

The radically different form of the effective potentials for static-field and microwave shielding will result in markedly different many-body physics. This will be true both for Bose-Einstein condensates of polar molecules and for polar molecules in optical lattices or tweezer arrays. For a sufficiently large number of particles and strong-enough Rabi coupling, microwave shielding is expected to result in a dense self-bound disc-like droplet [27, 28]. For large couplings, this may eventually undergo a transition into a crystalline monolayer of molecules [29]. In contrast, condensates of molecules shielded with static fields should (under proper conditions) form elongated filament-like droplets aligned along the direction of the field. These droplets, though resembling those observed in magnetic atoms [34], should not demand the stabilizing effect of quantum fluctuations. The properties of these self-bound droplets, including their stability, condensate fraction, and two-body correlations, are likely to be significantly different from those formed in the presence of microwave shielding. Condensates shielded with static fields may also present equilibrium multi-droplet solutions, which are not expected with microwave shielding [27, 29]. This will open intriguing questions about supersolidity [35] and pattern formation [36–38].

V. CONCLUSIONS

Ultracold polar molecules open up new frontiers for many-body physics. They provide experimentally realizable systems with strong dipole-dipole interactions, which challenge theories of dipolar quantum systems. However, ultracold molecules are stable only when protected from destructive short-range collisions by shielding methods. The interaction potentials offered by shielded ultracold molecules are different from the ones in common models. In particular, shielding produces interaction potentials with large repulsive cores, corresponding to repulsion at distances around 1000 bohr. This is very different from magnetic atoms, where the repulsion occurs at distances around 10 bohr and is fairly well represented by a contact (zero-range) interaction.

Simulations of condensed-phase or many-body behav-

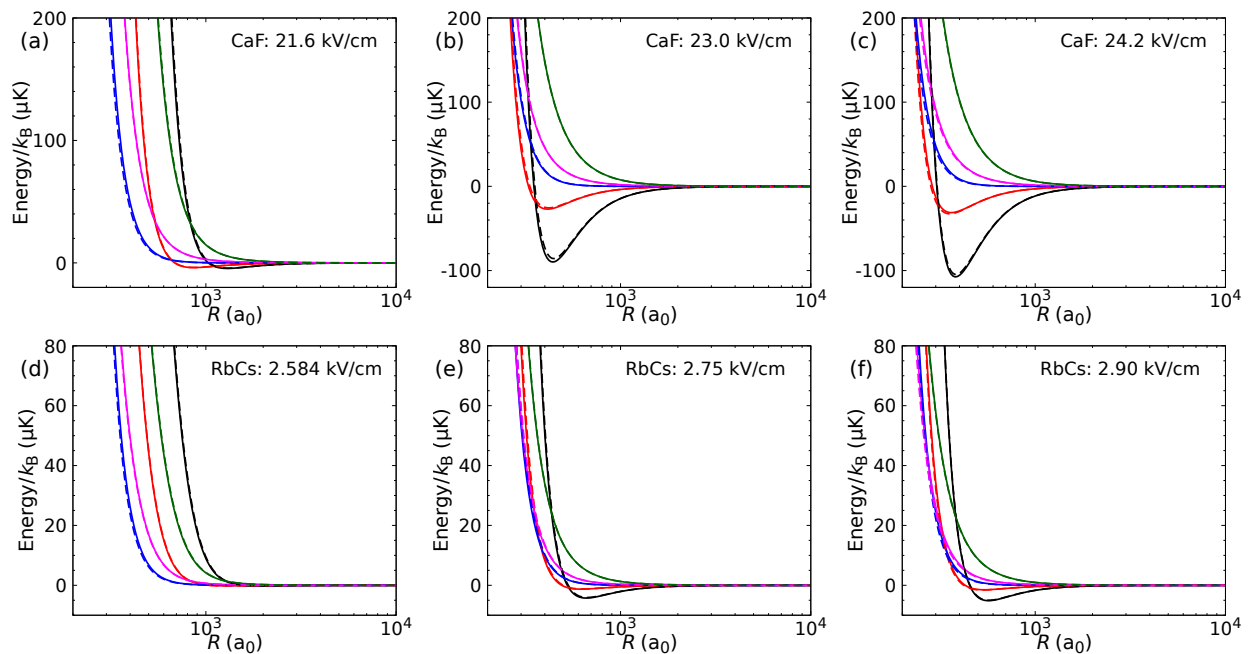


FIG. 9. Comparison of adiabats for CaF and RbCs in the initial pair state $(1,0)+(1,0)$, obtained from the fully coupled model of Eq. 27 (dashed lines) and from full matrix diagonalisation (solid lines). The values of \tilde{F} are the same as in Fig. 7.

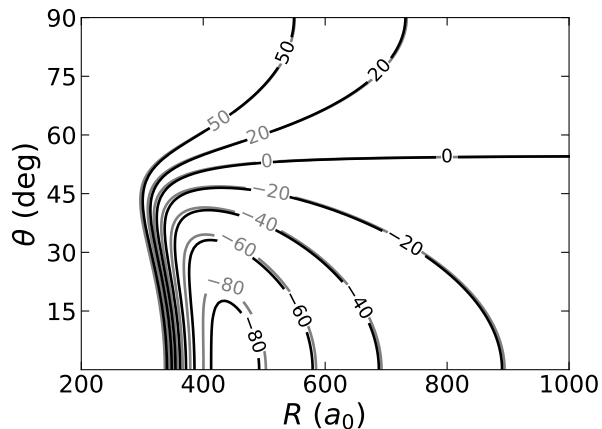


FIG. 10. Contour plot comparing $V_{\text{eff}}^{\text{fc}}$ (black lines) with adiabats obtained from full matrix diagonalisation (grey lines) for CaF at $F = 23$ kV/cm. Contours are labeled in μK and shown only up to $50 \mu\text{K}$.

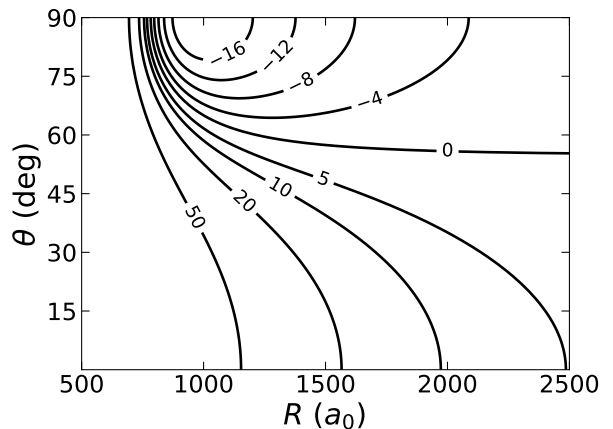


FIG. 11. Contour plot of effective potential for shielding of CaF with circularly polarised microwaves at Rabi frequency $\Omega = 30$ MHz and detuning $\Delta = 0$, using the functional form of ref. [24]. Contours are labeled in μK and shown only up to $50 \mu\text{K}$.

ior are computationally expensive. They require inexpensive ways to evaluate interaction potentials for each configuration. It is not computationally practical to diagonalize a substantial matrix at every point.

In this paper, we have examined the effective interaction potentials for pairs of ultracold molecules shielded from lossy collisions by static electric fields. We have derived forms of the effective potentials that can be evaluated efficiently and used in simulations of many-body

properties. We have compared our interaction potentials with previous ones that gave no attraction or repulsion near $\theta = 55^\circ$, and also with the ones appropriate for microwave shielding.

There is an important contrast between different types of shielding. Microwave shielding with circularly polarized fields gives effective potentials that are attractive for side-by-side geometries and favor molecules arranged

in two-dimensional sheets. Static-field shielding, by contrast, gives effective potentials that are attractive for end-to-end geometries and favor molecules in linear arrangements. Microwave and static-field shielding are thus complementary, and both are needed to explore the full range of many-body behavior that can exist.

RIGHTS RETENTION STATEMENT

For the purpose of open access, the authors have applied a Creative Commons Attribution (CC BY) licence to any Author Accepted Manuscript version arising from this submission.

DATA AVAILABILITY STATEMENT

The data that support the findings of this article are openly available from Durham University [at URL to be

supplied later]. A subroutine that evaluates the effective potentials efficiently is available from the authors on request.

ACKNOWLEDGEMENT

We are grateful to Michael Tarbutt for valuable discussions. This work was supported by the U.K. Engineering and Physical Sciences Research Council (EPSRC) Grant Nos. EP/P01058X/1 and EP/V011677/1. L.S acknowledges the support of the Deutsche Forschungsgemeinschaft (DFG, German Research Foundation) – Project-ID 274200144 – SFB 1227 DQ-mat within the project A04, and under Germany’s Excellence Strategy – EXC-2123 Quantum-Frontiers – 390837967).

-
- [1] L. De Marco, G. Valtolina, K. Matsuda, W. G. Tobias, J. P. Covey, and J. Ye. “A degenerate Fermi gas of polar molecules.” *Science*, **363**, 853 (2019).
- [2] G. Valtolina, K. Matsuda, W. G. Tobias, J.-R. Li, L. De Marco, and J. Ye. “Dipolar evaporation of reactive molecules to below the Fermi temperature.” *Nature*, **588**, 239 (2020).
- [3] A. Schindewolf, R. Bause, X.-Y. Chen, M. Duda, T. Karman, I. Bloch, and X.-Y. Luo. “Evaporation of microwave-shielded polar molecules to quantum degeneracy.” *Nature*, **607**, 677 (2022).
- [4] M. Duda, X.-Y. Chen, A. Schindewolf, R. Bause, J. von Milczewski, R. Schmidt, I. Bloch, and X.-Y. Luo. “Transition from a polaronic condensate to a degenerate Fermi gas of heteronuclear molecules.” *Nat. Phys.*, **19**, 720 (2023).
- [5] N. Bigagli, W. Yuan, S. Zhang, B. Bulatovic, T. Karman, I. Stevenson, and S. Will. “Observation of Bose-Einstein condensation of dipolar molecules.” *Nature*, **631**, 289 (2024).
- [6] L. Chomaz, I. Ferrier-Barbut, F. Ferlaino, B. Laburthe-Tolra, B. L. Lev, and T. Pfau. “Dipolar physics: a review of experiments with magnetic quantum gases.” *Rep. Prog. Phys.*, **86**, 026401 (2022).
- [7] A. Browaeys and T. Lahaye. “Many-body physics with individually controlled Rydberg atoms.” *Nat. Phys.*, **16**, 132 (2020).
- [8] D. K. Ruttley, T. R. Hepworth, A. Guttridge, and S. L. Cornish. “Long-lived entanglement of molecules in magic-wavelength optical tweezers.” *Nature*, **637**, 827 (2025).
- [9] R. Bause, A. Christianen, A. Schindewolf, I. Bloch, and X.-Y. Luo. “Ultracold sticky collisions: Theoretical and experimental status.” *J. Phys. Chem. A*, **127**, 729 (2023).
- [10] M. Mayle, G. Quémener, B. P. Ruzic, and J. L. Bohn. “Scattering of ultracold molecules in the highly resonant regime.” *Phys. Rev. A*, **87**, 012709 (2013).
- [11] A. Christianen, M. W. Zwierlein, G. C. Groenenboom, and T. Karman. “Photoinduced two-body loss of ultracold molecules.” *Phys. Rev. Lett.*, **123**, 123402 (2019).
- [12] A. V. Avdeenkov, M. Kajita, and J. L. Bohn. “Suppression of inelastic collisions of polar $^1\Sigma$ state molecules in an electrostatic field.” *Phys. Rev. A*, **73**, 022707 (2006).
- [13] G. Wang and G. Quémener. “Tuning ultracold collisions of excited rotational dipolar molecules.” *New J. Phys.*, **17**, 035015 (2015).
- [14] M. L. González-Martínez, J. L. Bohn, and G. Quémener. “Adimensional theory of shielding in ultracold collisions of dipolar rotors.” *Phys. Rev. A*, **96**, 032718 (2017).
- [15] J.-R. Li, W. G. Tobias, K. Matsuda, C. Miller, G. Valtolina, L. De Marco, R. R. W. Wang, L. Lassablière, G. Quémener, J. L. Bohn, and J. Ye. “Tuning of dipolar interactions and evaporative cooling in a three-dimensional molecular quantum gas.” *Nat. Phys.*, **17**, 1144 (2021).
- [16] B. Mukherjee, M. D. Frye, C. R. Le Sueur, M. R. Tarbutt, and J. M. Hutson. “Shielding collisions of ultracold CaF molecules with static electric fields.” *Phys. Rev. Res.*, **5**, 033097 (2023).
- [17] B. Mukherjee and J. M. Hutson. “Controlling collisional loss and scattering lengths of ultracold dipolar molecules with static electric fields.” *Phys. Rev. Res.*, **6**, 013145 (2024).
- [18] T. Karman and J. M. Hutson. “Microwave shielding of ultracold polar molecules.” *Phys. Rev. Lett.*, **121**, 163401 (2018).
- [19] L. Lassablière and G. Quémener. “Controlling the scattering length of ultracold dipolar molecules.” *Phys. Rev. Lett.*, **121**, 163402 (2018).
- [20] T. Karman and J. M. Hutson. “Microwave shielding of ultracold polar molecules with imperfectly circular polarization.” *Phys. Rev. A*, **100**, 052704 (2019).
- [21] T. Karman. “Microwave shielding with far-from-circular polarization.” *Phys. Rev. A*, **101**, 042702 (2020).

- [22] L. Anderegg, S. Burchesky, Y. Bao, S. S. Yu, T. Karman, E. Chae, K.-K. Ni, W. Ketterle, and J. M. Doyle. “Observation of microwave shielding of ultracold molecules.” *Science*, **373**, 779 (2021).
- [23] T. Karman, Z. Z. Yan, and M. Zwierlein. “Resonant and first-order dipolar interactions between ultracold $^1\Sigma$ molecules in static and microwave electric fields.” *Phys. Rev. A*, **105**, 013321 (2022).
- [24] F. Deng, X.-Y. Chen, X.-Y. Luo, W. Zhang, S. Yi, and T. Shi. “Effective potential and superfluidity of microwave-shielded polar molecules.” *Phys. Rev. Lett.*, **130**, 183001 (2023).
- [25] S. Yi and L. You. “Trapped atomic condensates with anisotropic interactions.” *Phys. Rev. A*, **61**, 041604(R) (2000).
- [26] S. Yi and L. You. “Trapped atomic condensates with dipole interactions.” *Phys. Rev. A*, **63**, 053607 (2001).
- [27] T. Langen, J. Boronat, J. Sánchez-Baena, R. Bombín, T. Karman, and F. Mazzanti. “Dipolar droplets of strongly interacting molecules.” *Phys. Rev. Lett.*, **134**, 053001 (2025).
- [28] W.-J. Jin, F. Deng, S. Yi, and T. Shi. “Bose-Einstein condensates of microwave-shielded polar molecules.” *Phys. Rev. Lett.*, **134**, 233003 (2025).
- [29] M. Ciardi, K. R. Pedersen, T. Langen, and T. Pohl. “Self-bound monolayer crystals of ultracold polar molecules.” (2025).
- [30] J. L. Bohn, M. Cavagnero, and C. Ticknor. “Quasi-universal dipolar scattering in cold and ultracold gases.” *New J. Phys.*, **11**, 055039 (2009).
- [31] L. Lassablière and G. Quéméner. “Model for two-body collisions between ultracold dipolar molecules around a Förster resonance in an electric field.” *Phys. Rev. A*, **106**, 033311 (2022).
- [32] J. H. Van Vleck. “On σ -type doubling and electron spin in the spectra of diatomic molecules.” *Phys. Rev.*, **33**, 467 (1928).
- [33] E. C. Kemble. *The Fundamental Principles of Quantum Mechanics*, (McGraw-Hill, New York, 1937).
- [34] H. Kadau, M. Schmitt, M. Wenzel, C. Wink, T. Maier, I. Ferrier-Barbut, and T. Pfau. “Observing the Rosensweig instability of a quantum ferrofluid.” *Nature*, **530**, 194 (2016).
- [35] F. Böttcher, J.-N. Schmidt, J. Hertkorn, K. S. H. Ng, S. D. Graham, M. Guo, T. Langen, and T. Pfau. “New states of matter with fine-tuned interactions: quantum droplets and dipolar supersolids.” *Rep. Prog. Phys.*, **84**, 012403 (2020).
- [36] J. Hertkorn, J.-N. Schmidt, M. Guo, F. Böttcher, K. S. H. Ng, S. D. Graham, P. Uerlings, T. Langen, M. Zwierlein, and T. Pfau. “Pattern formation in quantum ferrofluids: From supersolids to superglasses.” *Phys. Rev. Res.*, **3**, 033125 (2021).
- [37] Y.-C. Zhang, T. Pohl, and F. Maucher. “Phases of supersolids in confined dipolar Bose-Einstein condensates.” *Phys. Rev. A*, **104**, 013310 (2021).
- [38] M. Schmidt, L. Lassablière, G. Quéméner, and T. Langen. “Self-bound dipolar droplets and supersolids in molecular Bose-Einstein condensates.” *Phys. Rev. Res.*, **4**, 013235 (2022).